New Journal of Physics
The open access journal for physics

Structure formation in organic thin films observed in real time by energy dispersive near-edge x-ray absorption fine-structure spectroscopy

M Scholz[1,2], C Sauer[1,2], M Wiessner[1,2], N Nguyen[1,2], A Schöll[1,2,3] and F Reinert[1,2]

[1] Universität Würzburg, Experimentelle Physik VII, Am Hubland, D-97074 Würzburg, Germany
[2] Karlsruher Institut für Technologie (KIT), Gemeinschaftslabor für Nanoanalytik, D-76021 Karlsruhe, Germany
E-mail: achim.schoell@physik.uni-wuerzburg.de

New Journal of Physics **15** (2013) 083052 (14pp)
Received 19 March 2013
Published 27 August 2013
Online at http://www.njp.org/
doi:10.1088/1367-2630/15/8/083052

Abstract. We study the structure formation of 1,4,5,8-naphthalene-tetracarboxylicacid-dianhydride (NTCDA) multilayer films on Ag(111) surfaces by energy dispersive near-edge x-ray absorption fine-structure spectroscopy (NEXAFS) and photoelectron spectroscopy. The time resolution of seconds of the method allows us to identify several sub-processes, which occur during the post-growth three-dimensional structural ordering, as well as their characteristic time scales. After deposition at low temperature the NTCDA molecules are preferentially flat lying and the films exhibit no long-range order. Upon annealing the molecules flip into an upright orientation followed by an aggregation in a transient phase which exists for several minutes. Finally, three-dimensional islands are established with bulk-crystalline structure involving substantial mass transport on the surface and morphological roughening. By applying the Kolmogorov–Johnson–Mehl–Avrami model the activation energies of the temperature-driven sub-processes can be derived from the time evolution of the NEXAFS signal.

[3] Author to whom any correspondence should be addressed.

Contents

1. Introduction

Opto-electronic devices based on organic materials offer a variety of applications and have already entered the mass market [1, 2]. Such devices have in common that they are based on multiple layers of organic semiconducting materials. To optimize the crucial performance parameters, as e.g. the charge carrier mobility of the organic films, a comprehensive understanding of the interplay between film morphology, geometric structure and electronic structure is crucial. The growth of molecular films can be quite complex and generally a variety of parameters are of importance. Due to the anisotropic shape and internal degrees of freedom of molecules [3, 4], multiple thermally activated diffusion pathways and intermediate transient phases may occur during structure formation in condensates. The interlayer mass transport and additional energy barriers at step edges, the so-called Ehrlich–Schwoebel barriers [5, 6], determine the growth mode and the film morphology. For molecular systems, the height of such barriers depends on the orientation of the molecules and on the intermolecular interaction strength [7]. The complicated underlying physics makes it challenging to model and predict the structure formation in organic thin films. For a detailed understanding, specific case studies on well-defined model systems are thus mandatory. In particular, information on the processes involved in establishing the final structural arrangement, such as diffusion and the organization in transient phases, is highly desired, thus demanding experimental techniques with appropriate time resolution [8].

The π-conjugated planar molecules 1,4,5,8-naphthalene-tetracarboxylicacid-dianhydride (NTCDA), epitaxially grown on Ag(111) substrates are an eligible model system since they exhibit highly variable film growth depending on the growth rate and the substrate temperature as well as on post-growth annealing parameters. Preparation at substrate temperatures below 100 K results in smooth films with the molecules oriented nearly flat to the substrate surface. Moreover, no long-range order can be observed in low-energy electron diffraction measurements. Annealing at temperatures above 160 K changes the molecular orientation to almost upright standing [9, 10]. At the same time the films morphologically roughen and a lateral ordering can be observed, owing to the formation of three-dimensional crystalline islands with preferential azimuthal arrangement templated by the substrate. Hence, this is an ideal model system for the investigation of the dynamics of the structure formation with a time-resolved structural probe.

In this work we utilize energy dispersive near-edge x-ray absorption fine-structure spectroscopy (NEXAFS) with a time resolution in the range of a few seconds. This technique

allows us to monitor variations of the structural properties of the NTCDA films in real time. Three sub-processes can be identified, which occur during the formation of the stable film structure consisting of three-dimensional crystalline islands.

Before we discuss the experimental results we will in the following describe some experimental details and issues specific to data evaluation with energy dispersive NEXAFS.

2. Experimental

All experiments were performed in an ultra-high vacuum (UHV) chamber with a base pressure below 2×10^{-10} mbar. The Ag single-crystal preparation followed the standard sputtering and annealing procedure as described elsewhere [11]. The NTCDA films were prepared *in situ* by organic molecular beam deposition from a home-built Knudsen cell at a rate of about 0.2 monolayers (ML) per minute and at a substrate temperature of 95 K. The commercially available NTCDA was purified by sublimation twice prior to deposition. The film thickness was determined by the attenuation of the Ag 3d photoemission signal recorded with an Al-K_α x-ray source [12]. For accurate temperature determination during the temperature-dependent experiments, a thermocouple was mounted on the sample holder close to the sample. By cooling with liquid nitrogen and heating with a filament, sample temperatures between 95 and 800 K can be accessed and are stabilized by a proportional-integral-derivative (PID) controller. For filament currents below 4 A, which were sufficient to temperatures up to 230 K for the experiments presented in this work, no artifacts were observed in the NEXAFS and photoelectron spectroscopy (PES) data.

The experiments were performed at the beamline UE52-PGM of the BESSY II [10, 13]. The beamline can be operated in the traditional (i.e. energy scanning) and in an energy dispersive mode. By changing between two toroidal mirrors, the focus point of the synchrotron beam can be moved from the exit slit (energy scanning mode) to the sample surface (energy dispersive mode). In the energy dispersive mode, the exit slit is fully opened and does not limit the vertical spot size. The spot size in the energy dispersive mode is less than 50 μm in horizontal and about 3 mm in the photon energy dispersive vertical direction [13].

The width of the dispersive photon energy window and thus also the spatial separation of photon energies on the sample depends on the photon energy and on the fixed focus constant c_{ff}. For c_{ff} values larger than 7 and photon energies below 300 eV, the width of the dispersive photon energy window is nearly constant, i.e. $\Delta h\nu = 1.5$ eV. The c_{ff} value was consequently adapted in order to provide a sufficient signal-to-noise ratio while still avoiding radiation damage. For experiments in *multi-bunch hybrid mode*, c_{ff} values between 15 and 20 were utilized, while in *low-alpha multi-bunch hybrid mode* with lower ring current c_{ff} values were between 7 and 15. With such c_{ff} values a photon energy resolution of about 50 meV was derived at a sample current below 10 nA.

The NEXAFS spectra were recorded with at VG-SCIENTA R4000 electron analyzer, which is mounted at an angle of 55° to the incoming light with the entrance slit in the vertical direction. The analyzer can be operated in a *spatial imaging mode* (input lens 10× magnification applied here). The vertically dispersing light strip is thus mapped onto the two-dimensional channelplate detector while simultaneously resolving kinetic energies of the electrons in the horizontal direction. For a fast data acquisition, the so-called *fixed mode* of the analyzer was used with an energy window of about 15 eV. For C *K*-NEXAFS spectra of the C *KLL*-Auger electrons in the kinetic energy range between 252 and 267 eV were recorded.

With the described beamline and analyzer settings a C *K*-NEXAFS spectrum with a photon energy range of 1.5 eV and with a resolution of about 50 meV can be recorded within a few seconds. In addition, the UE52-undulator allows us to change the polarization of the incoming light from horizontal to vertical. In the utilized sample setup where the sample normal is horizontal and at an angle of 70° to the light, this translates into p- and s-polarization relative to the plane of incidence, respectively.

3. Data analysis

The NEXAFS data recorded in the dispersive beamline mode require a specific evaluation which differs in some details from the generally applied intensity normalization and energy calibration procedures for traditional NEXAFS. Most importantly, the data have to be corrected for spatially inhomogeneous response and nonlinear gain of the micro-channel plate (MCP), which will both immediately influence signal intensities and line shape. These issues are well known from (angle-resolved) PES experiments utilizing the same detectors [15, 16]. As a reference we measured the Ag *MNN*-Auger electron spectra with different photon flux in the analyzer's *fixed mode* and normalized the data to the sample current. Subsequently, a routine was calculated for each photon flux that corrects each MCP pixel so that the Ag *MNN*-Auger spectra match the respective data measured with a channeltron detector. All time-dependent NEXAFS data were also corrected for the constantly decreasing ring current. Also the photon energy calibration requires particular attention in dispersive NEXAFS. Usually, NEXAFS spectra are energy calibrated by determining the monochromator offset before or after the respective experiment from the well-known absorption lines of, e.g. gaseous samples such as N_2 or CO_2 [17–19], or from photoemission lines by using an electron analyzer [20]. These procedures cannot be directly applied to the dispersive NEXAFS data. We thus calibrated a NEXAFS spectrum recorded for a four-layer NTCDA/Ag(111) sample prepared at 95 K in the energy scanning mode with the photoemission signal of the Fermi edge according to [20]. This spectrum, which is displayed in figure 1(b), was then used for the calibration of the energy scale (see e.g. figure 1(c)). For all dispersive NEXAFS data reported in the following, the photon energy window of 284.75–286.3 eV was probed and an integration time of 6 s was used unless stated otherwise.

According to the calculations plotted at the bottom of figure 1(b), two main electronic transitions at the naphthalene ring system of NTCDA are probed in this energy window and thus contribute to feature B. These are denoted by C4 1s–$2\pi^*$ and C3 1s–$2\pi^*$ according to the respective core site (see also the molecular structure of NTCDA in the inset) and final state orbital (the second lowest unoccupied molecular orbital).

Note that since the monochromator and undulator are fixed in the energy dispersive mode, the relative accuracy of the photon energy axis during the experiment is very precise. Over the measurement time of a typical experiment of about 40 min, photon energy shifts due to instabilities are much smaller than 10 meV, which is demonstrated by the time-dependent data provided in figure 1(d). Relative energy shifts of NEXAFS signals of about 10 meV can thus be considered significant. The data in figure 1(d), which was recorded at a constant $T = 95$ K, also show that radiation damage cannot be observed within the typical experimental period of 45 min.

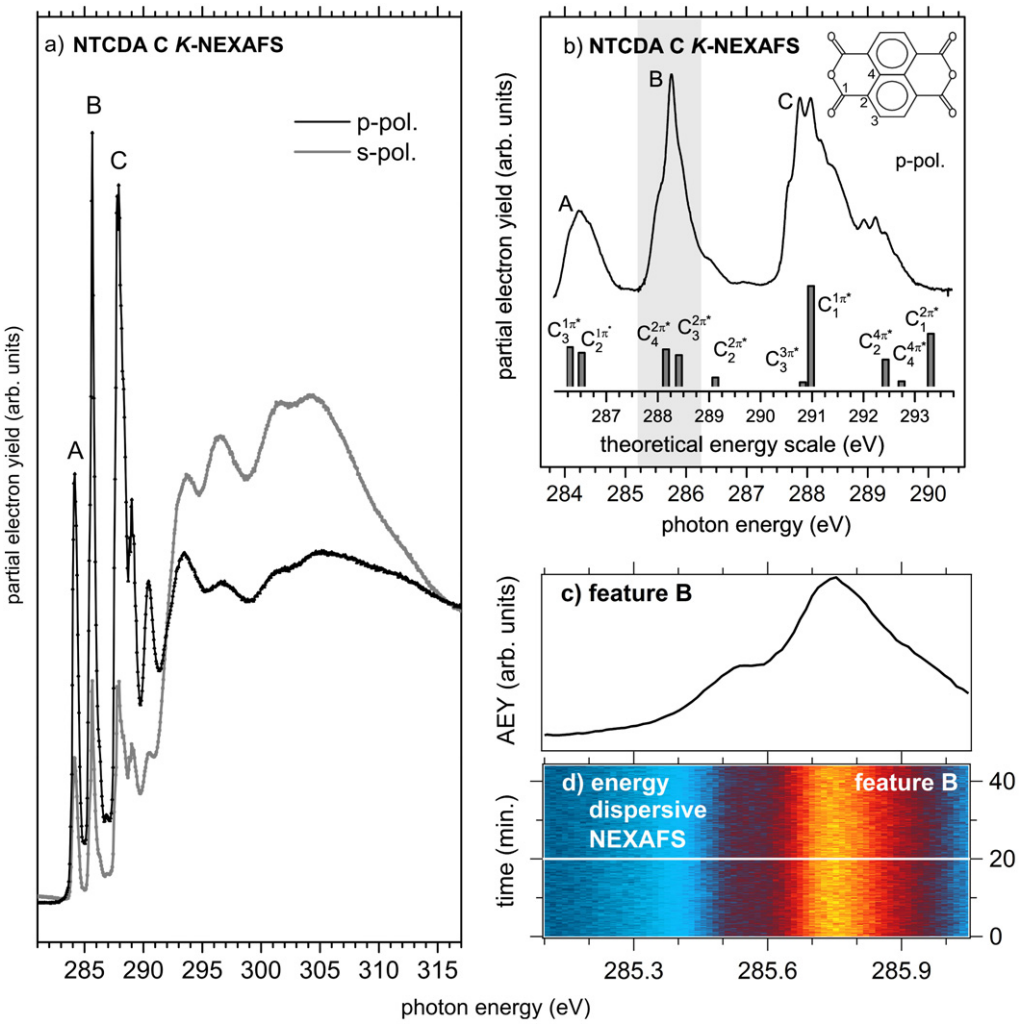

Figure 1. (a) C *K*-NEXAFS spectra of a NTCDA multilayer film prepared on Ag(111) at a sample temperature of 95 K. The spectra were recorded with s- and p-polarization in the traditional beamline mode. (b) π^*-region of the p-polarized spectrum plotted on an expanded energy scale. The most prominent signals are denoted by A–C and the shaded region indicates the photon energy window probed in the dispersive mode. At the bottom the result of an *ab initio* calculation is displayed [14]. Note that the theoretical energy scale was shifted and scaled to fit the experimental data. (c) NEXAFS signal of feature B recorded with p-polarization in the dispersive mode and averaged over 6 s. (d) Set of dispersive NEXAFS spectra recorded over about 45 min at a constant sample temperature of 95 K to demonstrate beamline stability and the absence of radiation damage. The white line at $t = 20$ min marks the position of the single spectrum plotted in (c).

4. Experimental results

The films investigated in the following post-growth study were all 8–10 ML thick and prepared at a substrate temperature of 95 K. This results in smooth films [9] with preferentially flat lying

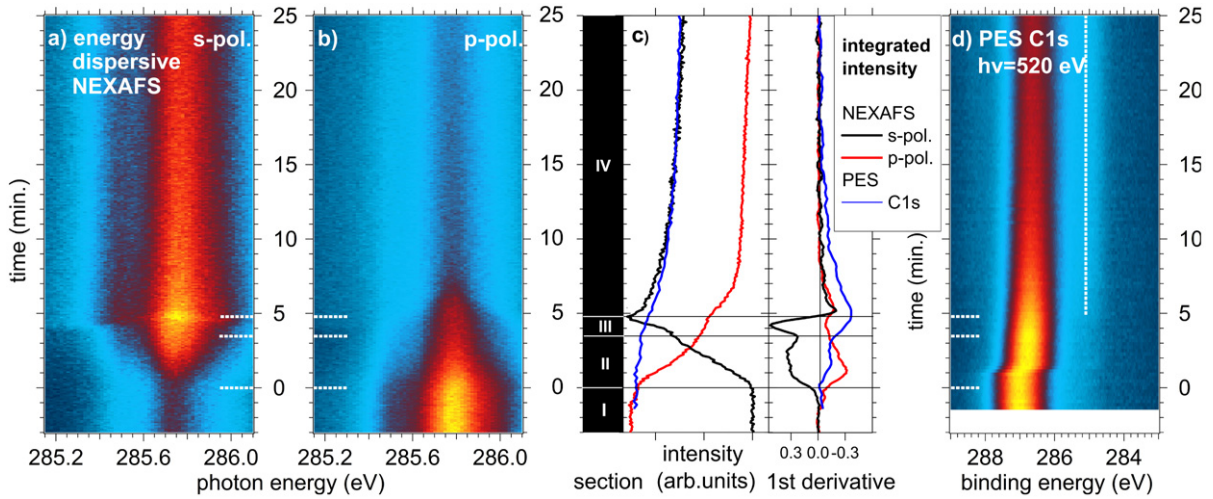

Figure 2. Time-dependent NEXAFS study of a NTCDA/Ag(111) sample (film thickness 8 ML, prepared at 95 K) after annealing to 200 K. The C *K*-NEXAFS spectra of feature B (see figure 1) recorded with s- and p-polarization of the incident light are displayed against time in color plots in (a) and (b), respectively. Yellow represents high, blue low intensity. The data acquisition was started after sample preparation at $t = -3$ min. The sample was heated quickly and at $t = 0$ a stable temperature of 200 K was established. (c) Integrated intensity (left) and first derivative (right) of NEXAFS feature B with s- (black) and p-polarization (red) derived from the data in (a) and (b), respectively. The general characteristics can be divided into four sections I–IV, as indicated on the left and by the black horizontal lines. The blue lines represent the C 1s intensity (integrated between 288.0 and 285.8 eV) and the first derivative, respectively, derived from the data in (d). (d) Time-dependent PES data of NTCDA/Ag(111) (film thickness 8 ML, prepared at 95 K) in the C 1s regime ($h\nu = 520$ eV), recorded up to 25 min after heating to 200 K. See text for details.

molecular orientation, as demonstrated by the strong linear dichroism [21] in the NEXAFS data presented in figure 1(a). Due to the symmetry selection rules for planar compounds such as NTCDA, strong (weak) absorption occurs for the C 1s–π^*-transitions if the $\vec{E}$-vector of the incoming light is perpendicular (parallel) to the molecular plane. Figure 2 shows the result of a time-resolved NEXAFS experiment in the dispersive mode, which monitors the transition from flat lying to upright standing molecules induced by annealing the films to 200 K. Figures 2(a) and (b) present sequences of NEXAFS spectra recorded with s- an p-polarization, respectively, in color plots. The data set starts after preparation at 95 K at $t = -3$ min. The sample was then quickly (i.e. in less than 1 min) heated to 200 K. $t = 0$ refers to the time when a constant temperature of $T = 200$ K was established. Figures 2(a) and (b) consistently show that annealing leads to an increase of the intensity of the NEXAFS feature B for s-polarization while at the same time a decrease for p-polarization occurs. This can immediately be associated with the expected change of the molecular orientation angle from flat lying to upright.

For a quantitative analysis of the time evolution, the intensity of NEXAFS feature B in figures 2(a) and (b) was integrated over photon energy and plotted against time in figure 2(c). For a better illustration of the intensity changes, the first derivatives of the integrated NEXAFS

signals are displayed on the right side of figure 2(c). Note that the data were normalized such that the ratio of the integrated intensity of feature B recorded with s- and p-polarization before annealing (i.e. at $t \leqslant -1$ min) corresponds well to the respective intensity ratio of the NEXAFS spectra obtained with the traditional setup (see figure 1(a)).

The curves in figure 2(c) show a very characteristic behavior that can be divided into four sections I–IV, as indicated on the left. In section I, i.e. after preparation and before the sample temperature has reached 200 K, the intensities in s- and p-polarization are constant, and the slope is consequently zero. Upon heating (section II) the intensity in p-polarization decreases, while it increases in s-polarization. Interestingly, the absolute values of the slope in s- and p-polarization are similar, until in section III the increase of signal in s-polarization is significantly stronger than the decrease in p-polarization. The respective time window between 3.5 and 4.8 min is small and delimited by a relatively sharp maximum of the intensity in s-polarization, which is followed by a parallel decrease of s- and p-polarized intensity with almost identical slope in section IV.

While the time evolution of the NEXAFS intensity in section II can be straightforwardly associated with a change of molecular orientation angle from flat lying to upright, sections III and IV immediately show that the post-growth annealing behavior of the NTCDA films is more complicated.

Additional information can be derived from time-dependent C 1s PES measurements, which are presented in figure 2(d). For the chosen photon energy of 520 eV, the kinetic energy of the photoelectrons and thus also the information depth of 2–3 ML [12] is similar to the case of the *KLL*-Auger electrons in the NEXAFS measurements. The experimental procedure was analogous to the NEXAFS analysis described above, i.e. the film (coverage 8 ML) was prepared at 95 K and subsequently annealed to a temperature of 200 K, which was established at $t = 0$ min. The color plot in figure 2(d) immediately shows a prominent shift of the energy position of the C 1s signal toward lower binding energy, which sets in after the sample has been at 200 K for about 1 min. Figure 2(d) furthermore demonstrates that the C 1s intensity decreases substantially in sections III and IV. The integrated intensity of the C 1s signal between 288.0 and 285.8 eV and the first derivative are compared with the respective curves derived from the NEXAFS data in figure 2(d) (blue curves). Note that the C 1s intensity curve was normalized to the intensity of the NEXAFS measurement with p-polarization at $t = 0$ and scaled to match the respective s-polarization curve at $t = 25$ min.

In section I the C 1s intensity is constant and the energy position is stable at 286.98 eV. In section II, however, a strong energy shift of about 230 meV toward lower binding energy occurs after the sample has been at 200 K for between 0.9–1.8 min. This is accompanied by a decrease of C 1s intensity as evidenced by the negative value of the respective first derivative. In the further time evolution the peak position shows an almost linear shift toward 286.63 eV at the end of section III and asymptotically approaches 286.52 eV in section IV. The intensity also decreases steadily, but shows the most prominent change at the transition between sections III and IV.

5. Interpretation and discussion

The combination of the NEXAFS and PES results in figure 2 allows a very detailed insight into the processes that occur upon annealing of the NTCDA films. As known from various spectroscopic [9, 22–25] and electron diffraction [26] investigations, the NTCDA multilayer

films are lacking long-range order after deposition at 95 K and can be considered amorphous. Moreover, the NTCDA molecules are preferentially oriented flat lying [9, 23] and the films are morphologically smooth, thus explaining the pronounced dichroism in the NEXAFS data (with larger intensity of the p-polarized signal) and the absence of any signal from the substrate interface in the PES data of figure 2 after preparation (section I). It is also established that annealing at temperatures above 160 K finally leads to films with crystalline islands [27], which refers to section IV of our time-dependent analysis. In this case the molecules are oriented preferentially upright with respect to the substrate [9], which is reflected by the inverted NEXAFS dichroism with now larger intensity in s-polarization. In addition, the enhanced crystallinity involves a morphological roughening of the films. Due to the limited probing depth of the PES and Auger electrons involved in our experiments, this leads to the decrease of the PES signal of the NTCDA multilayers observed in figure 2(d) and also to the collective decrease of the NEXAFS signals in s- and p-polarization illustrated in figure 2(c). The roughening furthermore accounts for the appearance of the C 1s signal of the first NTCDA layer, which is strongly bound to the Ag(111) substrate and is thus observed at lower binding energy in PES [24] (indicated by the vertical line between 10 and 25 min in figure 2(d)).

The formation of the three-dimensional islands with crystalline arrangement of the NTCDA molecules involves at least three sub-processes, which can be identified by our time-dependent analysis. If the substrate temperature is increased after preparation, the NTCDA molecules react at first by a change of the orientation angle from flat lying to upright. This is evidently shown by the inversion of the NEXAFS dichroism in section II. Note that the absolute values of the first derivatives of the s- and p-polarization signals are similar (figure 2(c)). At the same time the PES intensity is only very slowly decreasing, thus indicating only weak roughening of the films. The change of orientation angle is also reflected by the energy shift of the C 1s binding energy. Since the work function is constant at 4.95 ± 0.05 eV throughout the experiment, the energy shift entails a shift of the C 1s level with respect to the vacuum level. Moreover, also the valence levels shift rigidly with the core levels (not shown here). Such an effect has been observed before for similar systems and can be explained by the effect of the intramolecular charge distribution [28], leading to larger binding energies for flat lying than for upright standing aromatic compounds [29–31].

As soon as section II starts, the intensity patterns in figure 2(c) show a different evolution. While the NEXAFS signal in s-polarization is increasing even more strongly, the decrease in p-polarization is slowed down. At the same time the PES intensity starts to decrease, thus indicating the beginning of the roughening of the NTCDA film. Interestingly, this is accompanied by a significant alteration of the spectroscopic signature of NEXAFS feature B. We have previously reported on this change of line shape [10], which can be associated with a strong coupling of the NTCDA molecules in a transient phase. According to these findings, the molecules arrange in an upright configuration and with their molecular planes parallel during a confined time window of several minutes after annealing. Thickness-dependent experiments showed that this effect can be most clearly observed for films of less than 4 ML thickness.

Figure 3 demonstrates this transient phase for the example of a 5 ML NTCDA film in a time-dependent energy dispersive NEXAFS experiment with an analogous procedure to the experiments presented in figure 2. The color plot in figure 3(b) summarizes the time-dependent data set while in figure 3(a) several single NEXAFS spectra are compared, which have been deduced at the times indicated by the white dashed lines. After the sample has been at 230 K for about 4 min, the signature of feature B changes. Three relatively sharp signals arise which

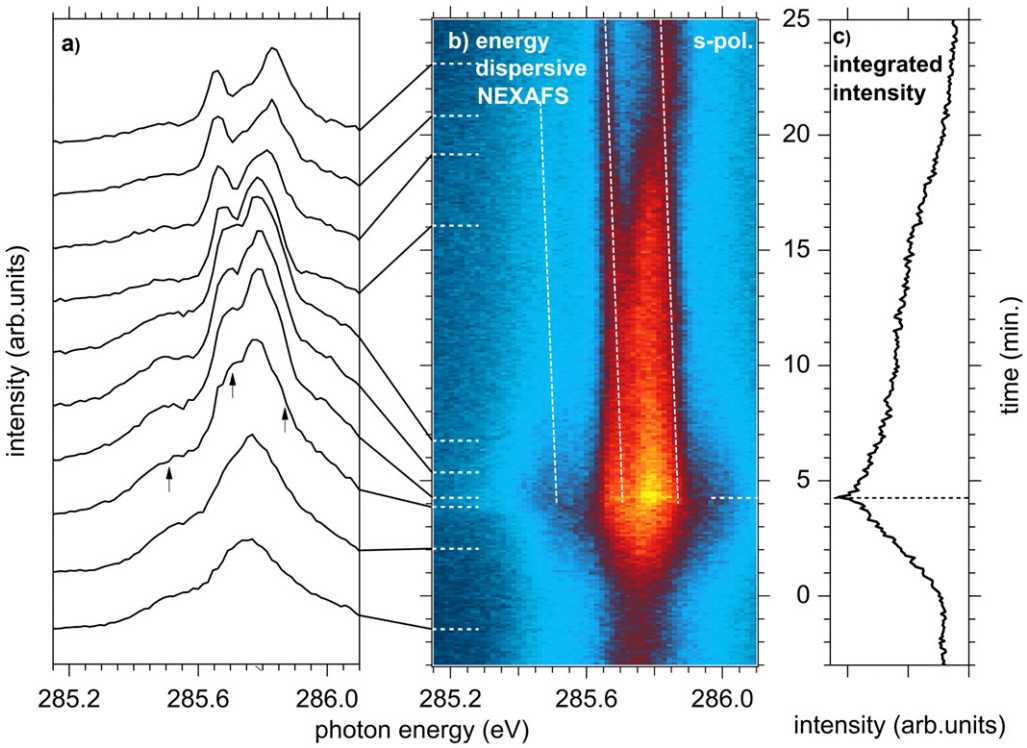

Figure 3. Time-dependent NEXAFS study of a 5 ML thick NTCDA film on Ag(111), prepared at 95 K, after annealing to 230 K. (a) Single C *K*-NEXAFS spectra of feature B deduced from (b) at the times specified by horizontal white lines (integration time 0.5 min). (b) Color plot of the energy dispersive C *K*-NEXAFS data of feature B recorded with s-polarization of the incident light. Yellow represents high, blue low intensity. The data acquisition was started after sample preparation at 95 K at $t = -4$ min. The sample was heated quickly and at $t = 0$ a stable temperature of 230 K was established. The dotted vertical white lines indicate the energy shift of specific peaks (indicated by black arrows in (a)), which are discussed in detail in the text. (c) Integrated intensity of NEXAFS feature B derived from the data in (b).

are indicated by the black arrows in figure 3(a). These sharp signals shift toward lower energy with time, which is also illustrated by the vertical dashed lines in figure 3(b). As elaborated in detail in [10] the strong coupling of the NTCDA molecules leads to a significant change of the vibronic profile and also the red-shift can be associated with this intermolecular coupling [10].

If we compare the time evolution of the intensity of feature B deduced from the experiment on the 5 ML thick NTCDA film in figure 3(c) with the respective curves for the 8 ML samples in figure 2(c), the similarities are striking. Of particular importance for our interpretation is the sharp intensity maximum in both data sets. This peak is a strong indication of the existence of the transient phase for samples with larger coverage.

We consequently suppose that the transient phase is established in the interface region, affecting about three layers on top of the strongly bound, flat lying first layer [24]. This also occurs for thicker films, where the topmost layers behave differently and do not show the spectroscopic signs of the strongly coupled transient phase. In consequence, in sections III

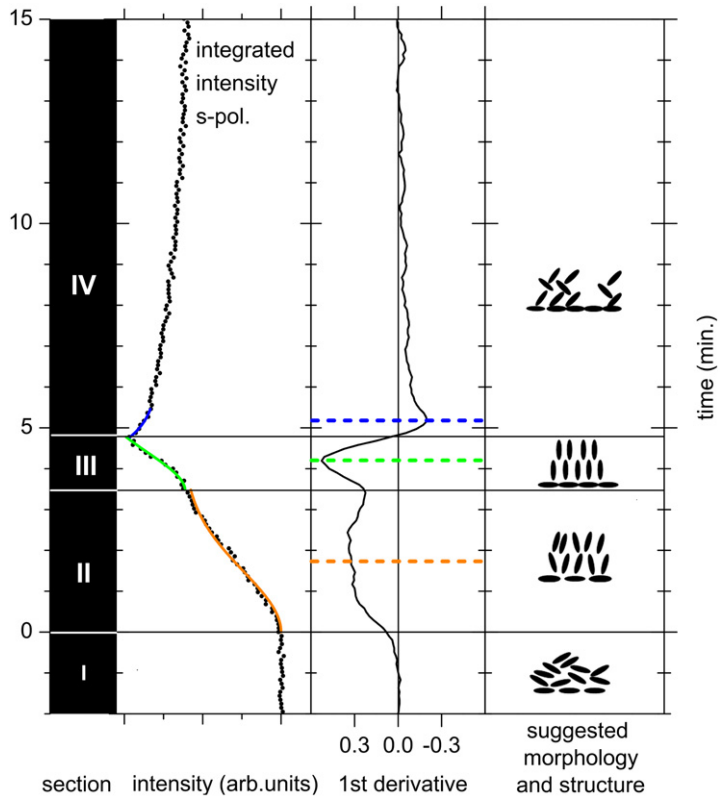

Figure 4. Illustration of the sub-processes involved in the post-growth structure formation of NTCDA films: intensity evolution of the integrated NEXAFS signal along with sigmoidal fits (orange, green and blue lines) in sections II–IV. Also the derivatives of the intensities of the NEXAFS and PES signals from figure 2(c) (left) together with sketches describing the structure and morphology in the respective sections I–IV are shown. The orange, green and blue dotted horizontal lines mark the maximum values of the slope, where 50% of the molecules are transformed during each phase transition. The respective values of the first derivative were used for the quantitative analysis of the activation energies (see text for details).

and IV the NEXAFS data of films thicker than 4 ML are a superposition of the transient phase and the topmost layers, which are upright standing and already arranged in crystalline islands.

In section IV the decrease of the intensities of the s- and p-polarization NEXAFS and the C 1s multilayer signals straightforwardly reveal that this regime is governed by a change of the film morphology. Obviously the organization of the molecules in three-dimensional islands is the dominating process, thus leading to an increasing roughening of the sample until a thermodynamically stable configuration is reached after about 25 min.

The picture of the post-growth annealing behavior of the NTCDA films, which we have drawn from our time-dependent analysis, is illustrated graphically by the sketches on the right-hand side of figure 4, together with the derivatives of the NEXAFS intensities from figure 2(c). Summarizing, three sub-processes occur. At first, the molecules change their orientation angle and flip into a more upright orientation. Then the NTCDA molecules aggregate into a transition

phase, featuring strongly coupled molecules with their molecular planes parallel to each other [10]. Finally, three-dimensional islands are formed with crystalline structure and marked roughening of the originally smooth films.

We have performed the same time-dependent NEXAFS experiments for several similar NTCDA samples after annealing to temperatures between 180 and 230 K. Interestingly, the time dependence of the NEXAFS signal is always similar and shows the same general characteristics as shown in figure 2(c) and described in detail above. However, the slope of the intensity patterns in each section shows a systematic dependence on temperature. For a quantitative analysis of the relevant sub-processes, we evaluated the intensity evolution in each section. If we assume an instant change of the molecular orientation, the NEXAFS signal is proportional to the number of molecules during each phase transformation. The observed characteristic intensity evolution can be best explained with the Kolmogorov–Johnson–Mehl–Avrami model. This model has proven to quite successfully describe the general kinetics in crystallization of amorphous materials, polymers, metals and metal alloys [32–35]. The phase transformation kinetics generally follows an 's'-curve, i.e. a sigmoidal type of function, from which kinetic parameters can be quantified.

For isothermal conditions and time-independent nucleation and growth rates, the transformed fraction x is given by

$$x(t) = 1 - \mathrm{e}^{-(kt)^n}, \tag{1}$$

where k is the temperature-dependent reaction rate constant, t the time and n the so-called Avrami exponent. In most situations, it can be assumed that the rate constant k shows an Arrhenius behavior

$$k = k_0 \mathrm{e}^{-\left(\frac{E_{\mathrm{act}}}{k_{\mathrm{B}}T}\right)}, \tag{2}$$

where k_0 is the frequency factor, E_{act} the activation energy and k_{B} the Boltzmann constant. With $f(x) = n(1-x)(-\ln(1-x))^{\frac{n^2-1}{n}}$ follows after the time derivative of equation (1), the expression

$$\ln\left(\frac{\mathrm{d}x}{\mathrm{d}t}\right) = \ln(k_0 f(x)) - \frac{E_{\mathrm{act}}}{k_{\mathrm{B}}T} \tag{3}$$

with the linear relation between $\ln\left(\frac{\mathrm{d}x}{\mathrm{d}t}\right)$ and the inverse of the absolute temperature $\frac{1}{T}$. By plotting $\ln\left(\frac{\mathrm{d}x}{\mathrm{d}t}\right)$ versus $\frac{1}{T}$ and assuming a constant frequency factor k_0 and Avrami's exponent n within a section, the activation energy for kinetic processes can be extracted from the slope of the respective curve.

For a quantitative analysis of the extrema of the slope, we fitted a sigmoidal type of function in each of the sections II–IV. In addition, we added a constant intensity offset to the fit function in sections III and IV, which was determined from the initial intensity at the beginning of the respective sections. In section IV we fitted an inverted 's'-curve to the intensity evolution, such that the extrema of the fit coincide with the minimum of the first derivative of the integrated NEXAFS signal. In figure 4 the fit functions in sections II–IV are plotted for the measurement at 200 K (orange, green and blue lines). In the following we will evaluate the extrema of the slope of the sigmoidal functions, which mark the time when 50% of the molecules are transformed during the phase transition. This positions are illustrated by the orange, green and blue dotted horizontal lines in figure 4.

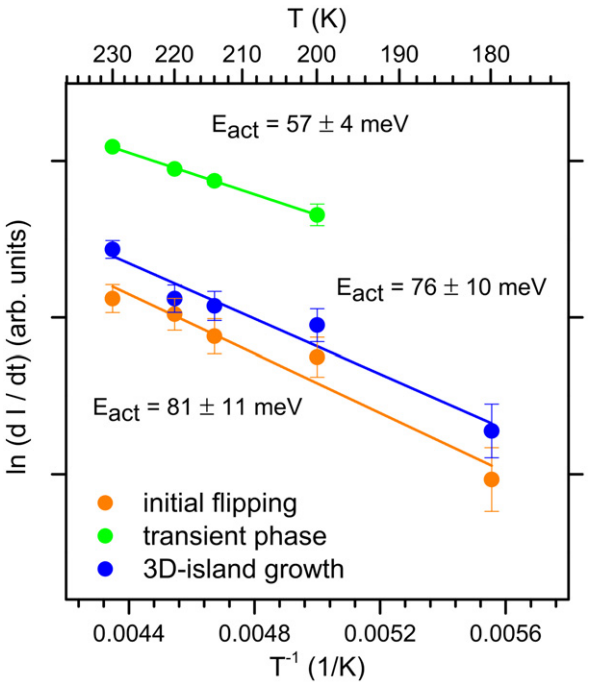

Figure 5. Arrhenius plot derived from the analysis of the time-dependent NEXAFS intensities. The values for the three different sub-processes flipping (orange), aggregation in a transient phase (green), and three-dimensional island growth (blue) show a linear behavior thus allowing a determination of the respective activation energies. Note that at 180 K the transient phase was not observed.

Figure 5 displays a plot of the result against the inverse temperature. A linear dependence of the values determined from the different sections can be clearly observed. From a linear fit the activation energies can be determined according to equation (3). The resulting values are 81 ± 11 meV for the initial flipping, 57 ± 4 meV for the transition into the transient phase and 76 ± 10 meV for the three-dimensional island growth.

6. Conclusion

We have studied the structure formation in molecular condensates on the example of NTCDA films on Ag(111). In this analysis we have applied and demonstrated the capabilities of energy dispersive NEXAFS. A particular advantage of this method is the simultaneous access to structural and spectroscopic (i.e. electronic structure) information with a time resolution of seconds. Moreover, it allows us to study the geometry and stability of transient phases which can be of crucial importance for the comprehensive understanding of film growth phenomena. This has been shown for various materials, from metals [36] to small molecules such as e.g. H_2O [37], were the geometric arrangement of the constituents follows a complicated dependence on the size of the aggregate or cluster.

The present study reports the first observation of analogous effects in the structure formation of large molecular compounds. During post-growth annealing of NTCDA multilayer

films, we identified different processes that occur prior to the formation of the crystalline films and we quantified the respective activation energies. After an initial flipping of the NTCDA molecules into a more upright orientation, a transient phase is established. The spectroscopic information simultaneously provided by the NEXAFS technique shows that the transient phase is characterized by a different electronic structure due to the particularly strong intermolecular coupling of the NTCDA molecules. Finally, on a time scale of several minutes three-dimensional islands are established with bulk-crystalline structure involving substantial mass transport on the surface and morphological roughening. By furthermore applying the Kolmogorov–Johnson–Mehl–Avrami kinetic growth model the respective activation energies were quantified.

Acknowledgments

We thank Patrick Hoffmann and the BESSY staff for assistance during beamtime. We acknowledge helpful discussions about the energy dispersive mode with David Batchelor. This work was financially supported by the Deutsche Forschungsgemeinschaft (DFG RE1496/9-1 and GRK 1221) and the Bundesministerium für Bildung und Forschung (contracts 03SF0356B).

References

[1] Fyfe D 2009 *Nature Photon.* **3** 453–5
[2] Volder M F L D, Tawfick S H, Baughman R H and Hart A J 2013 *Science* **339** 535–9
[3] Witte G and Wöll C 2004 *J. Mater. Res.* **19** 1889–916
[4] Schreiber F 2006 Organic molecular beam deposition: growth studies beyond the first monolayer *Physics of Organic Semiconductors* ed W Brütting (New York: Wiley-VCH) pp 15–40
[5] Schwoebel R L and Shipsey E J 1966 *J. Appl. Phys.* **37** 3682–6
[6] Schwoebel R L 1969 *J. Appl. Phys.* **40** 614–8
[7] Hlawacek G, Puschnig P, Frank P, Winkler A, Ambrosch-Draxl C and Teichert C 2008 *Science* **321** 108–11
[8] Kowarik S, Gerlach A, Sellner S, Schreiber F, Cavalcanti L and Konovalov O 2006 *Phys. Rev. Lett.* **96** 125504
[9] Gador D, Buchberger C, Fink R and Umbach E 1998 *Europhys. Lett.* **41** 231–6
[10] Scholz M, Holch F, Sauer C, Wiessner M, Schöll A and Reinert F 2013 *Phys. Rev. Lett.* **111** 048102
[11] Nicolay G, Reinert F, Schmidt S, Ehm D, Steiner P and Hüfner S 2000 *Phys. Rev.* B **62** 1631–4
[12] Graber T, Forster F, Schöll A and Reinert F 2011 *Surf. Sci.* **605** 878–82
[13] Batchelor D *et al* 2007 *Nucl. Instrum. Methods Phys. Res.* A **575** 470–5
[14] Kosugi N 1987 *Theor. Chem. Acc. Theory Comput. Modeling (Theor. Chim. Acta)* **72** 149–73
[15] Kay A W, Garcia de, Abajo F J, Yang S H, Arenholz E, Mun B S, Mannella N, Hussain Z, Van Hove M A and Fadley C S 2001 *Phys. Rev.* B **63** 115119
[16] Nordlund D, Garnier M G, Witkowski N, Denecke R, Nilsson A, Nagasono M, Mårtensson N and Föhlisch A 2001 *Phys. Rev.* B **63** 121402
[17] Tronc M, King G C and Read F H 1979 *J. Phys. B: At. Mol. Phys.* **12** 137–57
[18] Hitchcock A and Brion C 1980 *J. Electron Spectrosc. Relat. Phenom.* **18** 1–21
[19] Sham T K, Yang B X, Kirz J and Tse J S 1989 *Phys. Rev.* A **40** 652–69
[20] Scholl A, Zou Y, Schmidt T, Fink R and Umbach E 2003 *J. Electron Spectrosc. Relat. Phenom.* **129** 1–8
[21] Stöhr J 1992 *Nexafs Spectroscopy* (Berlin: Springer)
[22] Gador D, Buchberger C, Fink R and Umbach E 1998 *J. Electron Spectrosc. Relat. Phenom.* **96** 11–7
[23] Schöll A, Zou Y, Kilian L, Hübner D, Gador D, Jung C, Urquhart S G, Schmidt T, Fink R and Umbach E 2004 *Phys. Rev. Lett.* **93** 146406
[24] Bendounan A, Forster F, Schöll A, Batchelor D, Ziroff J, Umbach E and Reinert F 2007 *Surf. Sci.* **601** 4013–7

[25] Braatz C R, Öhl G and Jakob P 2012 *J. Chem. Phys.* **136** 134706
[26] Kilian L, Stahl U, Kossev I, Sokolowski M, Fink R and Umbach E 2008 *Surf. Sci.* **602** 2427–34
[27] Groh U 2007 *PhD Thesis* http://opus.bibliothek.uni-wuerzburg.de/volltexte/2007/2107/
[28] Duhm S, Heimel G, Salzmann I, Glowatzki H, Johnson R L, Vollmer A, Rabe J P and Koch N 2008 *Nature Mater.* **7** 326–32
[29] Chen W, Huang H, Chen S, Huang Y L, Gao X Y and Wee A T S 2008 *Chem. Mater.* **20** 7017–21
[30] Verlaak S, Beljonne D, Cheyns D, Rolin C, Linares M, Castet F, Cornil J and Heremans P 2009 *Adv. Funct. Mater.* **19** 3809–14
[31] Chen W, Qi D C, Huang H, Gao X and Wee A T S 2011 *Adv. Funct. Mater.* **21** 410–24
[32] Johnson W and Mehl R 1939 *Trans. Am. Inst. Min. Metall. Pet. Eng.* **135** 416
[33] Avrami M 1939 *J. Chem. Phys.* **7** 1103–12
[34] Avrami M 1940 *J. Chem. Phys.* **8** 212–24
[35] Avrami M 1941 *J. Chem. Phys.* **9** 177–84
[36] Eberhardt W 2002 *Surf. Sci.* **500** 242–70
[37] Johnston R L 2010 *Atomic and Molecular Clusters* (Boca Raton, FL: CRC)